

Effect of Pulse Frequency on Microstructural and Corrosion Properties of Inconel 718 Gas Tungsten Arc Weldments

N. Anbarasan¹ · S. Jerome¹ · Gandamalla Suresh¹ · R. Oyyaravelu²

Received: 18 September 2018 / Accepted: 15 February 2019 / Published online: 12 March 2019
© The Indian Institute of Metals - IIM 2019

Abstract A study has been carried out to understand the effect of pulse frequencies on the formation of laves phase, the microstructural and corrosion properties of Inconel 718. Bead on welds was made by using gas tungsten arc welding (GTAW) in pulsed mode at different frequencies such as 2, 4, 6, 8 and 10 Hz. Varying frequencies exhibit significant changes in weld surface ripples. Microstructural analysis revealed that the welds at 2, 4 and 6 Hz showed both columnar and equiaxed dendrite structure, while at 8 and 10 Hz, the welds predominantly had equiaxed dendrites. Scanning electron microscopy results showed a reduction in continuous laves phase with the increase in pulsing frequency. Corrosion studies confirmed that the pitting resistance was increased at a higher frequency due to the reduction in laves phase in welds.

Keywords Corrosion · Frequency · Laves · Ripples

1 Introduction

Inconel 718 is one of the most widely used precipitation-strengthened nickel-based superalloy in the aerospace industry. The fabrication of aerospace components extensively uses the GTAW process due to their ability to weld complex shapes and achieve quality welds. Welding in a

pulsed mode has many beneficial effects on the weld microstructure and mechanical properties [1, 2]. In GTAW, the weld quality is determined by the magnitude of ripple and humping of the solidified weld surface. These surface anomalies are closely related to the solute segregation, porosity, cracking and deformation of welds [3]. Surface morphology is one of the primary factors which influence the corrosion resistance of the welds [4]. According to Lucas [5], the weld bead morphology plays a vital role in minimizing the microfissuring. Though Inconel 718 have better weldability than other nickel-based superalloys, it is necessary to understand the effect of these surface irregularities on the mechanical and corrosion properties.

Formation of detrimental laves phases (Ni, Cr, Fe)₂(Nb, Mo, Ti) in the fusion zone is unavoidable in Inconel 718. The laves phase affects the mechanical properties of the welds. Therefore, it is essential to minimize the amount of laves phase [6, 7]. The formation of laves phase is prominent in a continuous current mode of GTAW which depletes the primary strengthening element niobium (Nb) in the matrix [8]. The brittle laves phases act as regions of crack initiation and propagation. Therefore, to achieve good weld properties, it is essential to reduce laves segregation. Hirata [9] reported that grain refinement offers a pathway to prevent solidification cracking, eliminate segregation of Nb and improve toughness. High-energy beam welding process such as laser and electron beam achieve grain refinement by enhancing the cooling rate due to its higher speed [10]. However, the problem persists in a GTAW process due to its higher heat input and manual welding process for complex structures.

Application of weld pool oscillation techniques such as pulsed mode of welding, an ultrasonic waveguide, pulsed shielding gas oscillation, vibrating filler, etc. in GTAW

✉ S. Jerome
jerome@nitt.edu

¹ Department of Metallurgical and Materials Engineering, National Institute of Technology Tiruchirappalli, Tiruchirappalli, Tamil Nadu 620015, India

² School of Mechanical Engineering, Vellore Institute of Technology, Vellore, Tamil Nadu 632014, India

induce grain refinement. McInerney et al. [11] achieved grain refinement through mechanically initiated weld pool oscillation. Among the different weld pool oscillation techniques, a current pulsing technique is the simplest form, which serves to be flexible and cost-effective in the industrial practice. Garland et al. [12] discussed the metallurgical advantage of current pulsing technique on the mechanical properties of welds. Janaki Ram et al. [13] conducted welding experiments with continuous current and pulsed modes of current on Inconel 718 and concluded that the later has a positive impact on the reduction in laves phase. Studies confirm that the amount of grain refinement varies as the pulse frequency varies [14].

The effect of the mid-range superimposed pulse frequencies (500–2 kHz) have been studied by Manikandan et al. [15] and they found that the increase in modulated frequency causes finer distribution of laves phase. Microstructural studies on mild steel by low-frequency current pulsing shows a transition from columnar to equiaxed grains [16]. Low-frequency range pulses are preferred during welding of pipes and thin sheets to avoid defects such as melt through, undercuts and overlaps [17]. Hence, lower frequency current pulsing has been used and its effects on the surface morphology and microstructure are investigated. Studies have reported that weld microstructures play a vital role on corrosion resistance of the weld [18, 19]. The passive layer of Ni and Cr oxides protects Inconel 718 welds, and current pulsing can alter the nature of the passive layer. Also, pitting corrosion resistance in Inconel 718 welds is affected by metallurgical changes and the presence of precipitates in the material [20]. This study primarily focuses on how the change in current pulsing frequency affects the grain growth and laves segregation. The subsequent changes in corrosion properties due to change in pulse frequencies are analyzed. A steep temperature gradient can also induces grain refinement in the welds. To achieve this condition, a small quantity (5 vol%) of hydrogen gas is mixed with argon gas. The Ar–H₂ mixture exhibits similar characteristics of helium gas. So, to minimize size of the laves phase, an attempt has been made to weld Inconel 718 by using combined effect of Ar–H₂ mixture shielding with current pulsing frequencies.

2 Experimental Procedure

2.1 Materials and Welding

A 2-mm-thick, Inconel 718 (Table 1) sheet in the solutionized (980 °C) condition was used for welding experiments. The material was cleaned and degreased with acetone before welding. A square wave-rectified DC-

pulsed power from Lincoln V205-T AC/DC welding equipment was used for welding. Bead on plate experiments were performed in pulsed mode welding with low-frequency pulses of 2, 4, 6, 8 and 10 Hz at a constant welding speed of 6 mm/s. Figure 1 shows the schematic of a pulse waveform in GTAW. The other welding parameters were maintained as constants throughout the investigation as tabulated in Table 2. Ishida [17] investigated the surface bead formation in pulsed GTAW, and these parameters were used in the present investigation. Ar (95%) + H₂ (5%) was used as a shielding gas as it provides a reducing atmosphere [21] and reduces the grain structure of the weld as reported by Anbarasan et al. [22]. Moreover, the Ar–5% H₂ mixture induces a steep temperature gradient, which induces the faster cooling rate. The samples were sectioned using a wire electrical discharge machining (WEDM) for other studies.

For metallographic studies, samples were mounted and polished by fine grit SiC emery sheets. The electrolytic etching was done using a 10% oxalic acid solution in water. The Dino-Lite digital microscope was used for macrostructure studies. The microstructures of the weldments were observed using a Leica optical microscope. Statistical and dimensional analysis of the weldment segregates, and bead morphology was done using Image J software. For the observation of the laves phase in the weldment, Carl Zeiss scanning electron microscope (SEM) with Oxford energy-dispersive X-ray spectrometry (EDS) was used. Vickers microhardness test was performed at a load of 500 g for a dwell time of 15 s on the weld surface.

2.2 Corrosion Test

Samples of size (15 × 6 × 2 mm) were sectioned from the weld top surface for corrosion tests. The corrosion test utilized a conventional three-electrode electrochemical cell. ACM gill potentiostat/galvanostat was used for the analysis of the signals from the electrolytic cell. A 3.5% aerated NaCl solution was filled in the test cell, and experiments were conducted as per ASTM G59 standards [23]. Cyclic potentiodynamic polarization tests were conducted at a scan rate of 1 mV/s. For better accuracy of the results, experiments were repeated thrice with freshly prepared electrolyte.

3 Results and Discussion

3.1 Surface and Cross-Sectional Morphology

Figures 2 and 3 show the bead surface and cross-sectional morphology of welds obtained by different pulse frequencies. It is observed that current pulsing has considerable

Table 1 Inconel 718 elemental composition (in wt%)

Fe	Cr	Nb	Mo	Ti	Al	Co	C	Mn	Si	P	S	B	Cu	Ni
19.62	18.5	4.84	3.14	1.03	0.552	0.076	0.057	0.084	0.076	0.006	0.010	0.003	0.021	Rem

Fig. 1 Schematic of pulse waveform at low and high frequency in pulsed GTAW process

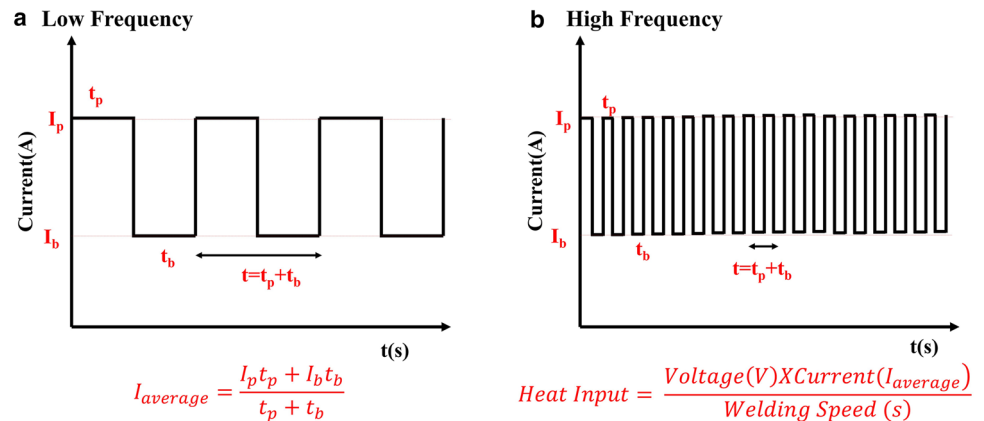


Table 2 Welding parameters

Pulse frequency	Peak current (I_p)	Background current (I_b)	Duty cycle (%)	Ar (95%) + H ₂ (5%) – Shielding gas L/min	Torch speed (mm/s)	Electrode diameter (mm)	Arc voltage (V)	Heat input (J/mm)
2	90	15	50	15	6	1.6	13 ± 0.3	113.75
4	90	15	50	15	6	1.6	13 ± 0.3	113.75
6	90	15	50	15	6	1.6	13 ± 0.3	113.75
8	90	15	50	15	6	1.6	13 ± 0.3	113.75
10	90	15	50	15	6	1.6	13 ± 0.3	113.75

influence on the weld bead appearance. Topographical analysis of the weld bead shows *ripple* formations, and it is prominent for all pulsing frequencies. However, humping and gouging are absent in all welds. The occurrence of ripples on the surface increases with the increased frequency. These ripples are caused by the weld pool oscillation induced during current pulsing [24]. The plasma arc column induces a high pressure in the center of the weld pool surface. However, pressure around the center is lower than which causes depression as depicted in Fig. 4a. This pressure difference enables the weld pool to stretch and acts as a membrane during peak current cycle. When the cycle changes to background current (I_b) in the weld pool, the plasma pressure is released. Such fluctuation in pressure causes the weld pool surface to retrace towards the center, thereby initiating an oscillation motion. With the absence of physical force owing to the moving arc, the oscillations continue till the weld pool solidifies. When the welding is performed by pulsed mode, the plasma pressure

varies according to the magnitude of the current as well as its frequency. Such fluctuation of pressure causes the weld pool oscillation. A high peak (I_p)-to-background (I_b) current ratio is used to provide a maximum arc pressure fluctuation between the pulsing cycle which induces a significant weld pool oscillation.

The partially penetrated weld pools oscillate in two modes as shown in Fig. 4b where ‘mode 1’ has contraction and expansion motion, while ‘mode 2’ is called as sloshing mode (Fig. 4c), which is caused by constant fluctuation of the molten pool from one side to another [11]. The oscillation frequency of the weld pool depends on the magnitude of the surface tension and density of the weld pool. For a weld pool of constant diameter, based on the mode of oscillation, the frequency of the weld pool varies [25]. Since the weld pool frequency influences the solidification structure, it is essential to identify the mode of oscillation which has been induced in the weld pool [26]. From the macrographs (Fig. 3), the mode of oscillation can be

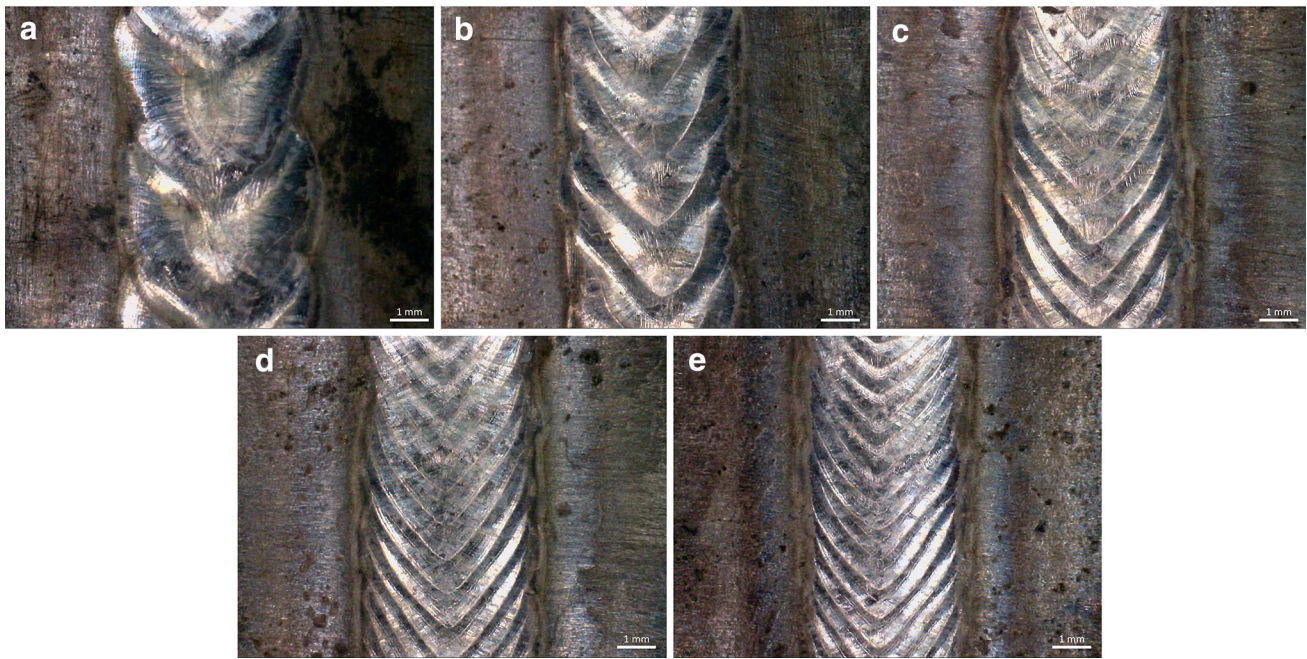


Fig. 2 Surface ripples due to current pulsing at **a** 2 Hz, **b** 4 Hz, **c** 6 Hz, **d** 8 Hz and **e** 10 Hz

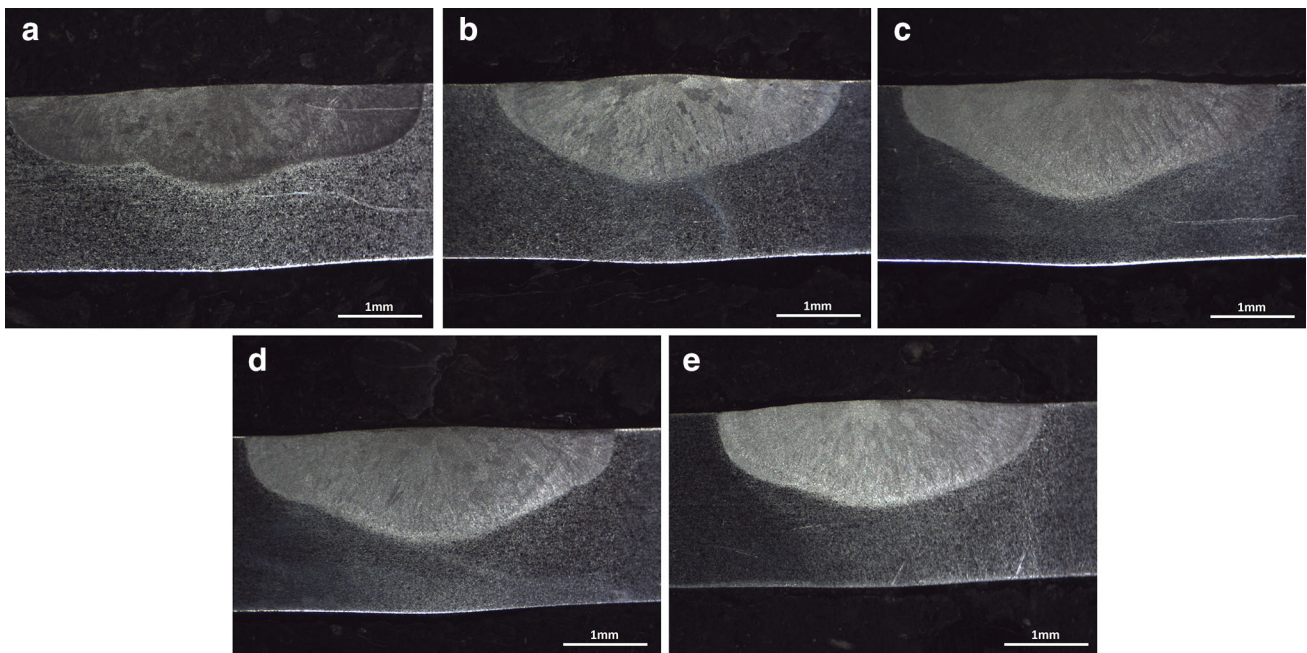


Fig. 3 Transverse cross-sectional bead morphology at **a** 2 Hz, **b** 4 Hz, **c** 6 Hz, **d** 8 Hz and **e** 10 Hz

recognized. It is observed that the weld beads are symmetrical and elliptically shaped which conforms to ‘mode 1’ oscillation. Table 3 lists the weld bead dimensions of all welds concerning change in current pulsing. The graphical plot (Fig. 5) of bead dimensions reveals that the bead width decreases with the increases in pulse frequency, while the variation of depth of penetration is insignificant with respect to pulse frequencies.

The aforementioned changes in the bead geometry are caused by the change in the weld pool convection. It is mainly driven by electromagnetic force, surface tension, plasma flux and buoyancy. However, during current pulsing, the electromagnetic force is considered as a prime driver of convection, and the flow is directed from the weld pool boundary towards the center [27]. As the frequency in the current pulsing varies, the rate of convective flow in the

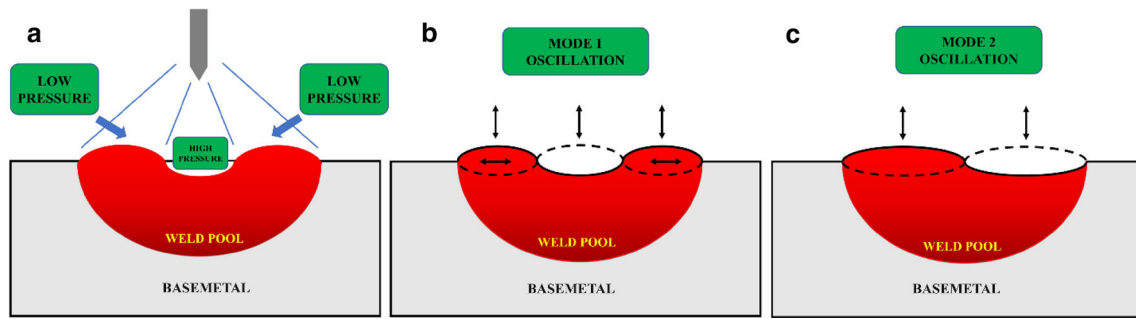


Fig. 4 Schematic of **a** arc pressure in pulsed GTAW, **b** mode 1 and, **c** mode 2 weld pool oscillation

Table 3 Bead dimensions and weld pool frequency

Arc (Hz)	Diameter ($\times 10^{-3}$ m)	Depth of penetration ($\times 10^{-3}$ m)	Pool frequency (Hz)
2	4.7	1.15	288
4	4.0	1.23	366
6	3.9	1.39	375
8	3.9	1.31	376
10	3.6	1.23	420

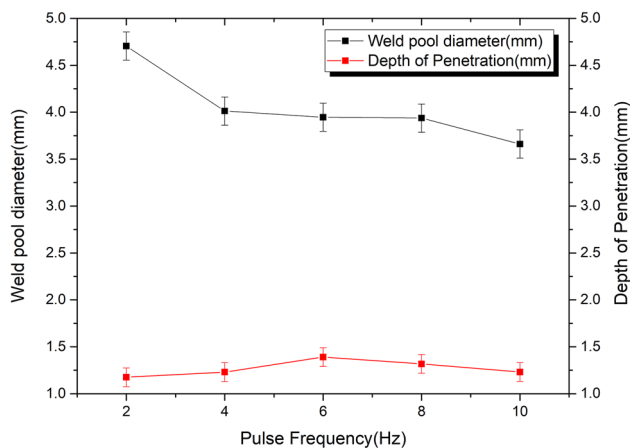


Fig. 5 Pulse frequency influence on bead geometry

weld pool also varies. The bead width decreases with an increase in frequency due to the lack of convective flow in the weld pool edges. Furthermore, the weld pool solidification is initiated during the background current period (t_b) due to lower heat input. In addition to lower heat input, the background current of 2 Hz pulsing has a longer time interval (250 ms) than the 10 Hz (50 ms). This longer time interval at lower pulse frequencies allows the weld pool to solidify much faster which prevents the convective flow towards the center, and therefore, the weld pool width is increased.

3.2 Microstructural Analysis

Macrographs (Fig. 6) reveal the variation in grain structure by varying frequencies. Figure 7a shows the 980 °C solution-annealed base metal microstructure with annealing twins and NbC at grain boundaries. HAZ microfissuring is not observed in any of the welds, and the grain growth starts from the PMZ as observed in Fig. 7b. Figure 8 is an example of a microfissure-free HAZ weld obtained at 2 Hz. Figure 9 shows the microstructural features of the weld and HAZ at various pulse frequencies. For a 2 Hz pulsing, columnar grains are observed from the fusion line (Fig. 9a) to the weld center, while equiaxed dendrites are scarcely present at the weld center (Fig. 9f). At 4 Hz, columnar grains are observed in the fusion line (Fig. 9b) and grain structure changes to equiaxed grains at the weld centerline (Fig. 9g). While at 6 Hz, the columnar grains initiate from the partially melted grains of the fusion zone (Fig. 9c), but a shorter distance away, their growth is terminated, and equiaxed grains (Fig. 9h) are present.

Grain refinement involves dendritic fragmentation followed by heterogeneous nucleation and grain growth. For 8 Hz and 10 Hz, microstructures are predominantly composed of fine equiaxed dendrites, and the columnar grains are scanty near the fusion line. From the micrographs, it is evident that in pulsed GTAW, the growth of columnar grains to equiaxed grains (columnar to equiaxed transition-CET) has been enhanced by increasing pulsing frequency. This transition can be attributed to the periodic change in the energy input with 195 J/mm during peak current I_p and 32.5 J/mm during background current I_b amounting to an average heat input of 113 J/mm (Table 2). In the present experiments, peak-to-background current ratio is 50%, which results in peak current time of 250, 125, 83, 62 and 50 ms for 2, 4, 6, 8 and 10 Hz. Since thermal fluctuation is controlled by current pulsing, the rate of fluctuation depends on the pulse frequency. Higher pulse frequencies cause faster thermal fluctuations than lower frequencies. These temperature variations can cause the growing dendrites to remelt and break off at the solidification front, and

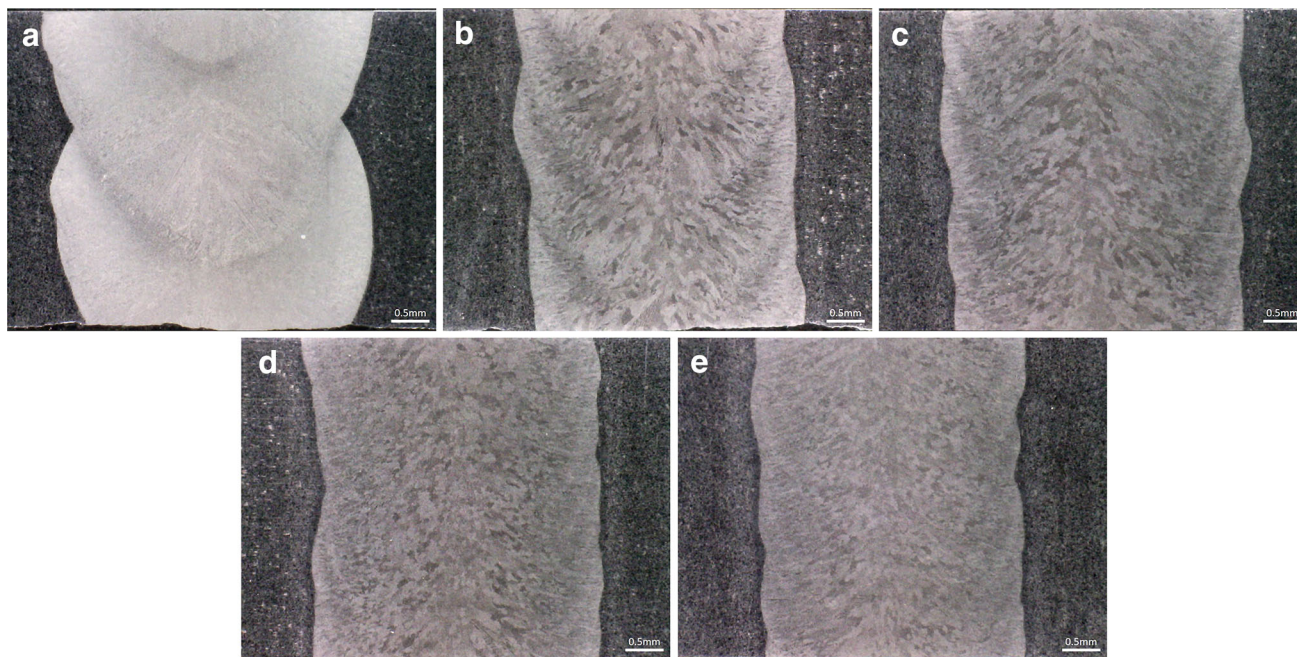


Fig. 6 Weld surface macrographs at **a** 2 Hz, **b** 4 Hz, **c** 6 Hz, **d** 8 Hz and **e** 10 Hz

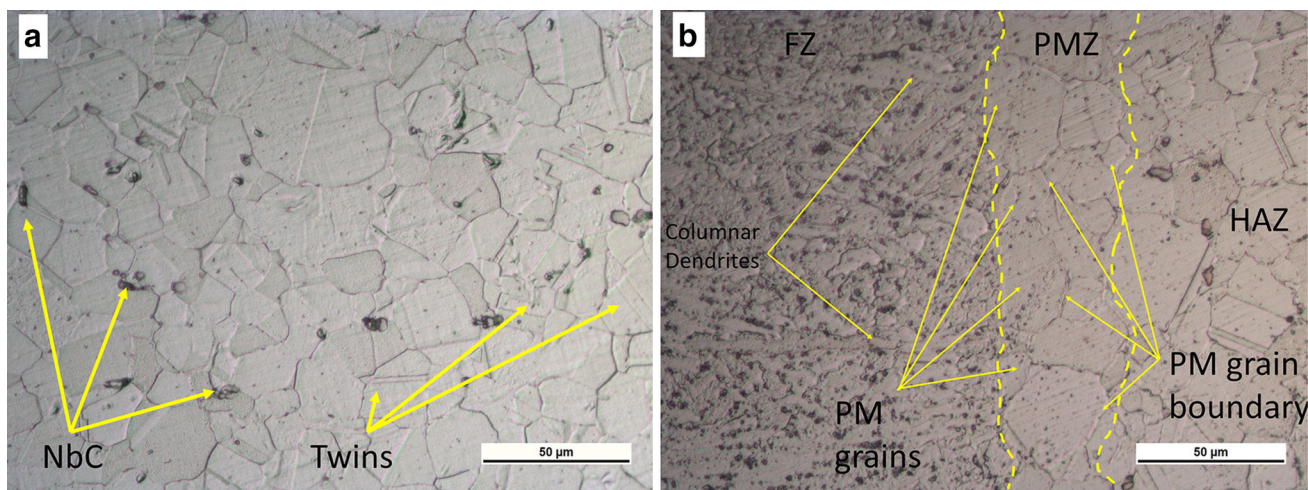


Fig. 7 Microstructures of **a** base metal and **b** PMZ

the broken dendrite tips act as sites of heterogeneous nucleation.

Also, the weld pool oscillation induced by current pulsing can also aid in the distribution and break up these dendrites to achieve grain refinement as reported by McInerney et al. [11]. Since the oscillating weld pool expands and contracts, it also assists in fragmentation of the dendrites. The size of the weld pool determines the frequency at which it oscillates. Xiao et al. [25] derived a mathematical relation to calculate the weld pool oscillation frequency of pulsed GTAW during solidification from the diameter of the weld pool as mentioned below for the partial penetration ‘mode 1’:

$$f = 5.84 \sqrt{\frac{\gamma}{\rho}} D^{-\frac{3}{2}} \quad (1)$$

where f is the weld pool oscillation frequency (Hz), γ is the surface tension of the weld pool (Nm), ρ is the density of the weld pool (kg/m^3) and D is the diameter of the weld pool (m). D value is equivalent to the width of the weld bead from the macrographs. This relation is used in the current investigation to find the oscillation frequency of the weld pool. The γ (1.882 Nm) and ρ (7400 kg/m^3) values from ASM handbook [28] at $1336 \text{ }^\circ\text{C}$ are used in Eq. 1 to determine the oscillation frequency of the weld pool at the final stages of solidification. Figure 10 reveals how weld

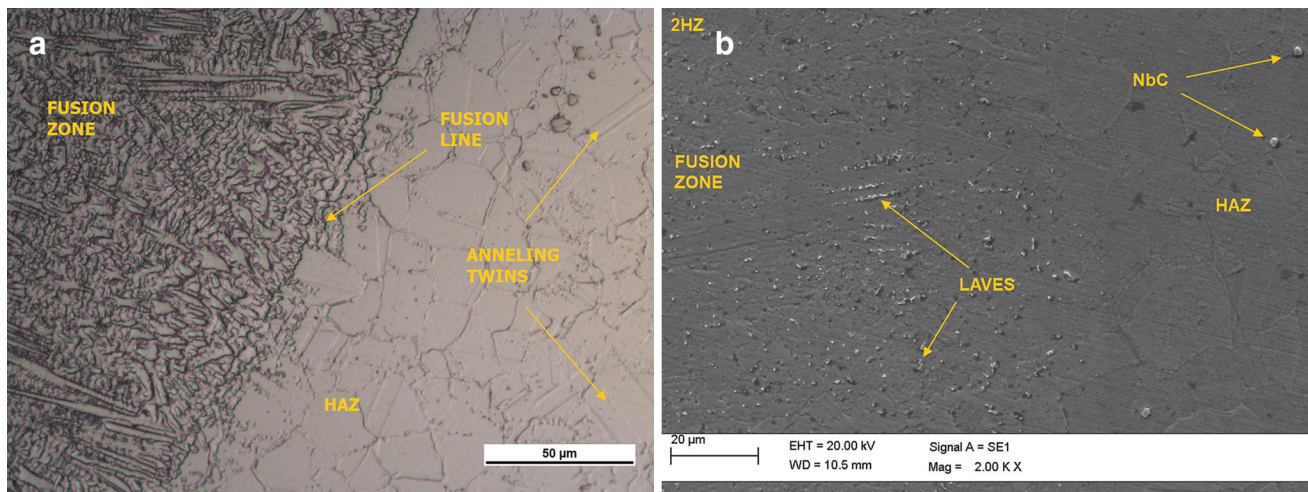


Fig. 8 Microfissuring-free HAZ at 2 Hz **a** OM and **b** SEM

pool oscillation varies with current pulsing, and it specifies that an increase in pulse frequency improves the weld pool oscillation. This higher pool frequency breaks the columnar dendrites to equiaxed dendrites and enhances the distribution of the dendritic fragments.

The results can be correlated with the micrographs observed at 8 and 10 Hz. The presence of more equiaxed grains indicate a large dendritic fragmentation. These fragments move ahead of the solidifying interface, while the reduced thermal gradients assist them in their survival. However, at 2 Hz, the fragmented dendrite's survival is not possible due to a higher temperature gradient. Also, current pulsing elevates the cooling rates and reduces the thermal gradients which cause an undercooling effect in the weld pool. Therefore, equiaxed dendritic growth is sustained. Moreover, the long solidification range (1250–1330 °C) of Inconel 718 assists in a larger mushy zone formation which makes the dendritic fragmentation more effective [29]. The columnar grains largely present at 2 Hz indicate that the weld experience lower cooling rate while the equiaxed grains formed at 10 Hz indicate that a higher cooling rate is achieved. The transition from predominant columnar to equiaxed grains with an increase in current pulsing frequency indicates an enhancement of cooling rate.

3.3 Laves Phase Distribution

The eutectic laves phase formation in alloy 718 is inevitable during the terminal phase of solidification. During solidification, Inconel 718 undergoes the following reactions: $L \rightarrow \gamma + L \rightarrow (\gamma + NbC) + L \rightarrow \gamma + L \rightarrow \gamma + Laves$. However, the amount of NbC is negligible in the fusion zone owing to the very low carbon content [30]. The solidification condition immensely influences laves phase

constitution and distribution in the weld microstructure. Irrespective of the pulsing frequencies, laves phase segregation is observed in the interdendritic regions, of the welds. Figure 11 shows that the laves phase characterized using SEM/EDS analysis is visible in the form of white clusters. The line scan results of laves phase display a compositional change across dendritic core with Nb (15 wt%) and Mo (12 wt%) content higher than the base metal composition. It confirms that laves phase depletes the Nb and Mo from the dendritic core regions, thus reducing its solid solution strengthening effects [8]. In this study, laves phase distribution in the fusion zone is analyzed for the various pulse frequencies and Fig. 12 shows laves distribution in fusion zones of all the welds. Image threshold analysis has been used to measure the amount of laves phase over an area of 2200 μm^2 along the weld centerline for all the pulsing frequencies. Researchers have used image analysis techniques to analyze laves phase size and distribution. The size of laves phase obtained by Manikandan et al. [31] is 6–13 μm^2 , while Anbarasan et al. [22] have achieved laves size of 7–12 μm^2 in GTAW of Inconel 718 by using Ar–5% H_2 .

A histogram plot to study the distribution of these laves phase over various ranges is shown in Fig. 13. The histogram plots reveal that the amount of laves phase decreases with an increase in pulse frequency. Continuous interconnected laves phase with a size range of 2–3.2 μm^2 is observed in 2 Hz welds. In addition, they also have a significant amount of laves with size less than 2 μm^2 . At 10 Hz, very fine discrete laves of size lower than 2 μm^2 are observed indicating a decrease in size with an increase in pulse frequency. The fraction of laves phase is reduced from 8.2 to 3.7% with an increase in pulse frequency from 2 to 10 Hz. The morphological change and distribution of

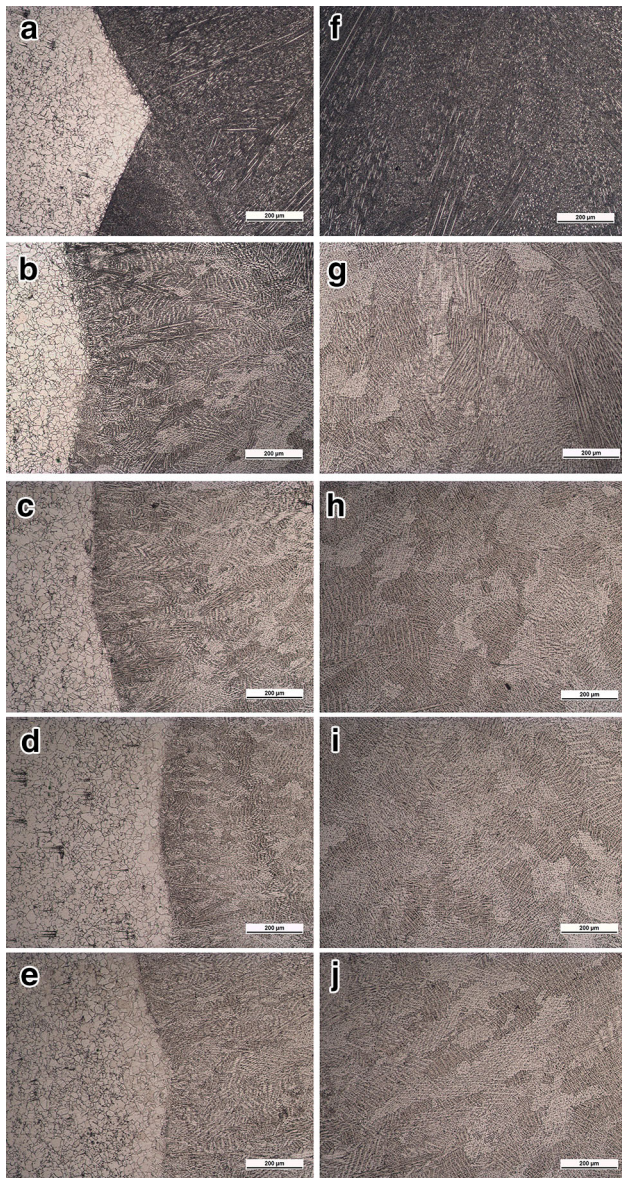


Fig. 9 Microstructures of HAZ **a** 2 Hz, **b** 4 Hz, **c** 6 Hz, **d** 8 Hz, **e** 10 Hz and centerline, **f** 2 Hz, **g** 4 Hz, **h** 6 Hz, **i** 8 Hz, **j** 10 Hz

laves phase can be attributed to the enhanced cooling rates in the weld due to the increase in pulse frequency. At higher frequency, the equiaxed grain formation results in a very small dendritic arm spacing distance compared to lower frequency pulsing. The reduced dendritic arm spacing lowers the size of the segregated laves phase. Vishwakarma et al. [32] reported similar enhancement of cooling rates and subsequent reduction in laves segregation due to a reduction in the dendritic arm spacing distance. Therefore, continuous interconnected laves phases are observed at 2 and 4 Hz, where columnar grains are present while equiaxed microstructure of 6, 8 and 10 Hz shows a

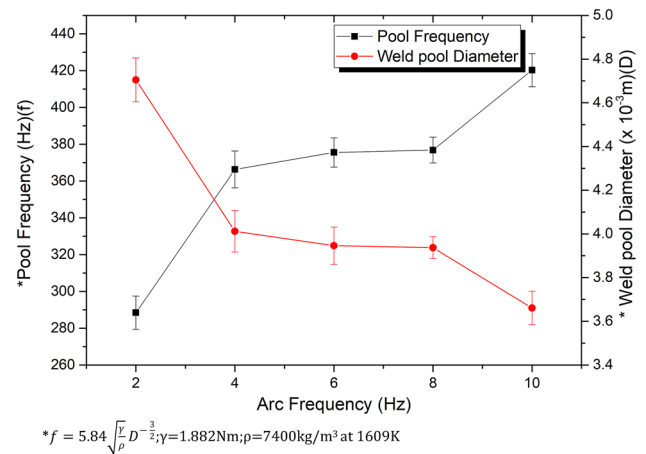


Fig. 10 Weld pool oscillation frequency due to current pulsing

finely isolated laves phase. Also, the continuous laves require higher post-weld solutionizing temperature to attain better mechanical properties by dissolution of laves phase. However, this causes severe grain coarsening in the weldment [8]. The presence of fine isolated laves at a higher pulsing frequency can favor easier dissolution at lower temperatures. Hence, problems associated with higher heat treatment temperatures such as surface oxidation, deformation and grain coarsening of the components can be minimized.

3.4 Microhardness

Vickers microhardness measurements are along the centerline and transverse section on the surface of the weld pool. Figure 14a shows the transverse microhardness plot of all the pulsing frequencies and fusion zone displays the highest hardness. However, no significant differences in microhardness values are observed due to current pulsing. The average microhardness values of the fusion zone is around 245 Hv, and the base metal has a value of around 225 Hv. A microhardness gradient plot (the difference between two adjacent hardness points) reveals (Fig. 15) the uniformity of grain refinement along the weld centerline. Yang et al. [33] pointed out similar grain refinement phenomenon in Ti alloy. For 2, 4 and 6 Hz, there is more fluctuation in the microhardness gradient which indicates a nonuniform microstructural growth. The nonuniformity is attributed due to the presence of columnar and equiaxed grains. The fluctuation in microhardness reveals the presence of continuous laves phases in these weld surfaces. Manikandan et al. [31] reported similar instances of an increase in surface microhardness due to the formation of continuous laves phase. Laves phase reduces the concentration of strengthening elements like Nb and Mo in the

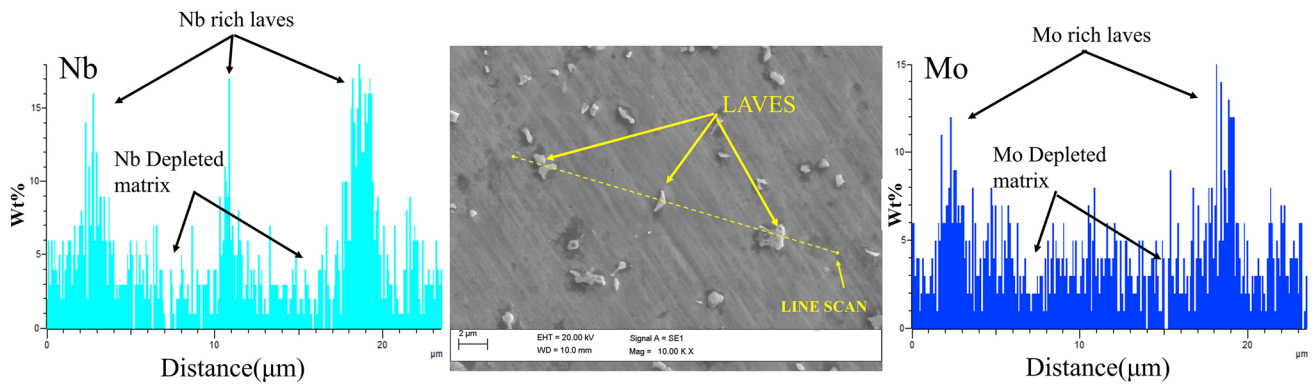


Fig. 11 Line scan across the laves

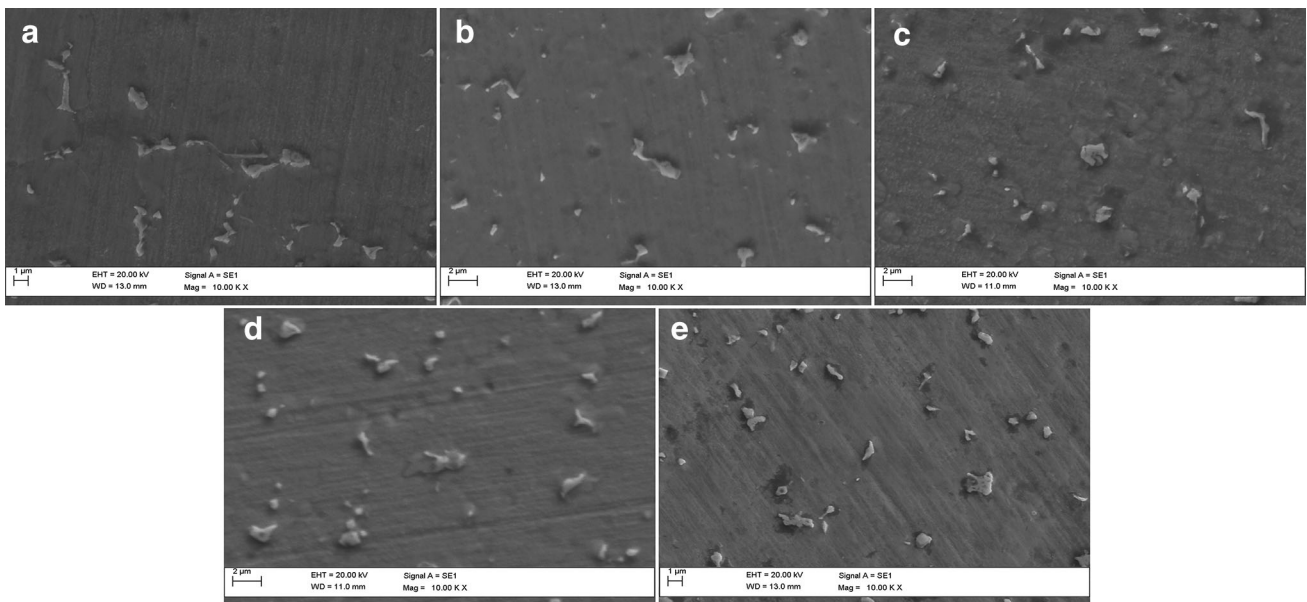


Fig. 12 SEM of laves phase at **a** 2 Hz, **b** 4 Hz, **c** 6 Hz, **d** 8 Hz and **e** 10 Hz

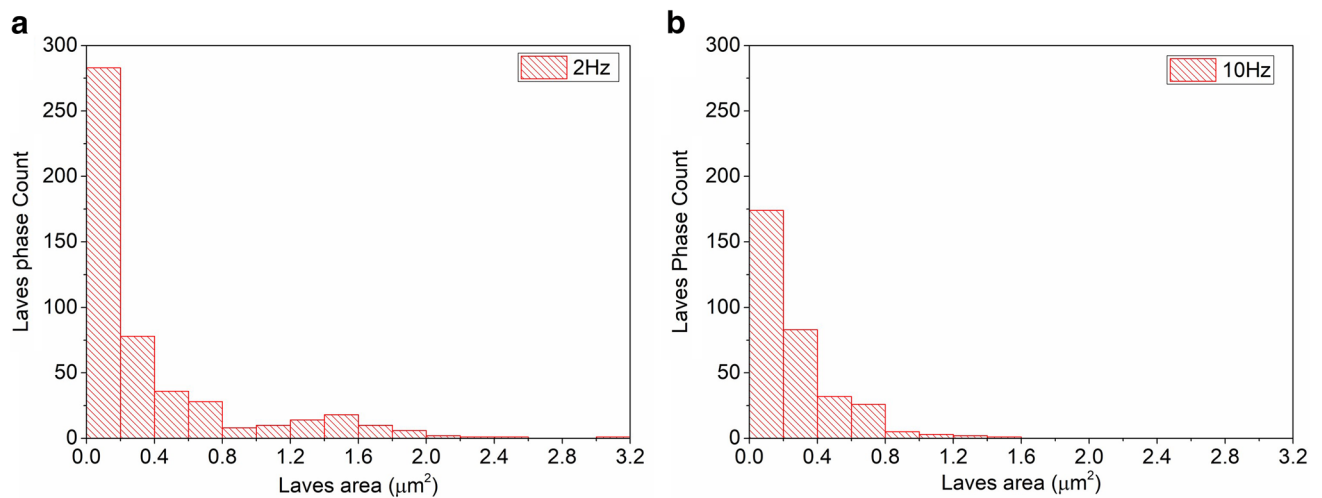


Fig. 13 Histogram of laves phase amount at **a** 2 Hz and **b** 10 Hz

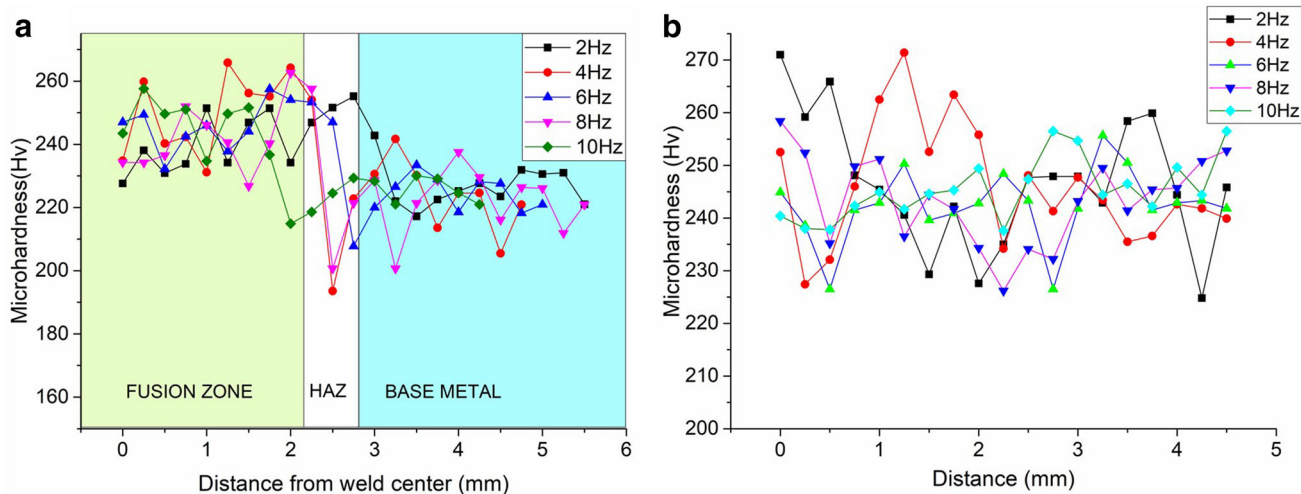


Fig. 14 Microhardness plot at transverse and centerline of weld surface

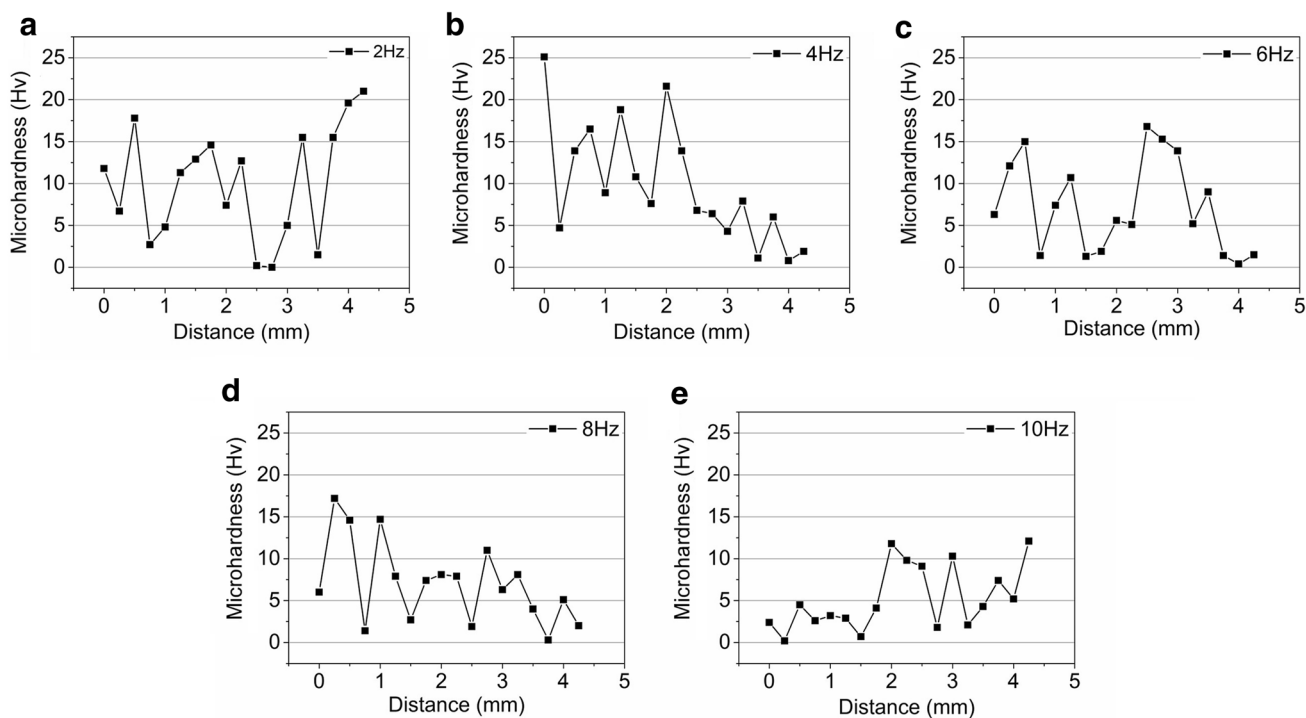


Fig. 15 Microhardness gradient at weld centerline for **a** 2 Hz, **b** 4 Hz, **c** 6 Hz, **d** 8 Hz and **e** 10 Hz

matrix; thus, microhardness in these regions is reduced [34]. While welds obtained using 8 and 10 Hz minimal fluctuations in the microhardness gradient are observed due to lower laves, segregation and the same has been confirmed by the SEM results (Figs. 12, 13). Hence, it confirms that the grain refinement is achieved at higher frequencies.

3.5 Corrosion

The cyclic potentiodynamic polarization plots for fusion zones of 2, 4, 6, 8 and 10 Hz in 3.5% NaCl solution are shown in Fig. 16. Table 4 presents the calculated electrochemical parameters such as i_{corr} , E_{corr} , E_{pit} , E_{rep} and hysteresis loop area of all the specimens. The passivation behavior is entirely different for all welds at all pulse

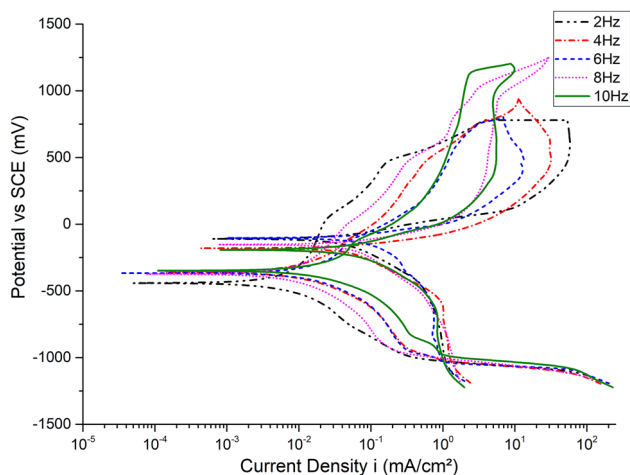


Fig. 16 Cyclic PDP curves of 2, 4, 6, 8 and 10 Hz frequencies

frequencies. The results indicate that the changing current frequencies do not significantly influence the i_{corr} values. However, the change in E_{corr} values is significant for all the specimens.

The E_{corr} values increases with the increases in the pulse frequency with the lowest being -440mV_{SCE} for a 2 Hz pulse frequency, while for the 10 Hz pulsing, it has an E_{corr} value of -351 mV_{SCE} . This variation in the E_{corr} value indicates that the change in frequency has affected the behavior of the passive protective layer on the weld surface. Inconel 718 has a protective outer and an inner passive layer for resistance against corrosive species [35]. Nobler E_{corr} values for higher frequencies indicate a well-protected homogenous passive layer. The outer passive layer is predominantly of Ni and Fe oxides and hydroxides while the inner barrier layer is of chromium oxide [35]. Pitting occurs when this passive layer fails to breakdown, allowing easier penetration of the Cl^- ions from the electrolyte. The potential is reversed after pit initiation at a reversal current (i_r) of 33.9, 6.9, 12.5, 20 and 9 mA/cm^2 for 2–10 Hz samples. A higher E_{pit} value pitting indicates higher resistance to pitting and the $E_{pit} - E_{corr}$ values indicate the probability of pit initiation. Both E_{pit} and

$E_{pit} - E_{corr}$ values indicate that the pitting resistance of the welds is in the order $10\text{ Hz} > 8\text{ Hz} > 6\text{ Hz} > 4\text{ Hz} > 2\text{ Hz}$. E_{rep} is the repassivation potential where the anodic curve is intersected during the reverse cycle. Hysteresis loop area between the E_{rep} and E_{pit} indicates the repassivation behavior of the pits. Smaller loop area better indicates better repassivation tendency of the pits. From the results, the welds made at 10 Hz have a smaller area compared to 2 Hz, and the hysteresis loop area is in the order $10\text{ Hz} < 8\text{ Hz} < 6\text{ Hz} < 4\text{ Hz} < 2\text{ Hz}$.

Gooch [36] stated that the stability of the passive layer is affected by the local compositional variations arising during solidification of the weld pool. As reported in the previous section, laves phase distribution is not uniform across the pulse frequencies, and thus the chemical homogeneity is not uniform for all pulsing frequencies. The higher resistance to pitting offered at 10 Hz can be attributed to the fine microstructure and reduced laves fraction (3.7%). Andre et al. [37] reported that the presence of laves phase in stainless steels reduces the pitting corrosion resistance. Laves reduces the Nb concentration in the matrix (2–3 wt%) as observed from the EDS line scans which are lower compared to the base material (4.84 wt%). Cardoso et al. [38] reported that higher concentration of elements like Nb and Mo improves the pitting corrosion resistance in austenitic stainless steels. However, in the current investigation, the depletion of Nb and Mo indicates a loss of corrosion resistance around the laves area. Siska et al. [34] reported an improvement in the pitting resistance with an increase in Nb content in austenitic stainless steel. The pitting resistance of 2 Hz pulse frequency weld is lower than 10 Hz due the continuous laves network and high laves fraction (8.2%). SEM (Fig. 17) of the corroded samples indicate a larger pit size at 2 Hz in the matrix than 10 Hz. At 10 Hz, the amount of Nb-depleted matrix is lowered due to fine laves. Thus, an increase in pulse frequency improves the pitting resistance of the Inconel 718 welds.

Table 4 Corrosion parameters measured from Tafel analysis

Frequency Hz	E_{corr} mV_{SCE}	i_{corr} $\mu\text{A}/\text{cm}^2$	E_{pit} mV_{SCE}	$E_{pit} - E_{corr}$ mV_{SCE}	Hysteresis area Coulomb (C)
2	-440 ± 10	10.16 ± 2	765 ± 5	1205	$2.06 \pm .01$
4	-360 ± 10	14.32 ± 3	848 ± 7	1208	$1.18 \pm .01$
6	-370 ± 10	14.62 ± 1	880 ± 10	1250	$0.39 \pm .01$
8	-374 ± 10	10.13 ± 2	1084 ± 10	1458	$0.36 \pm .01$
10	-351 ± 10	11.80 ± 1	1139 ± 4	1490	$0.30 \pm .01$

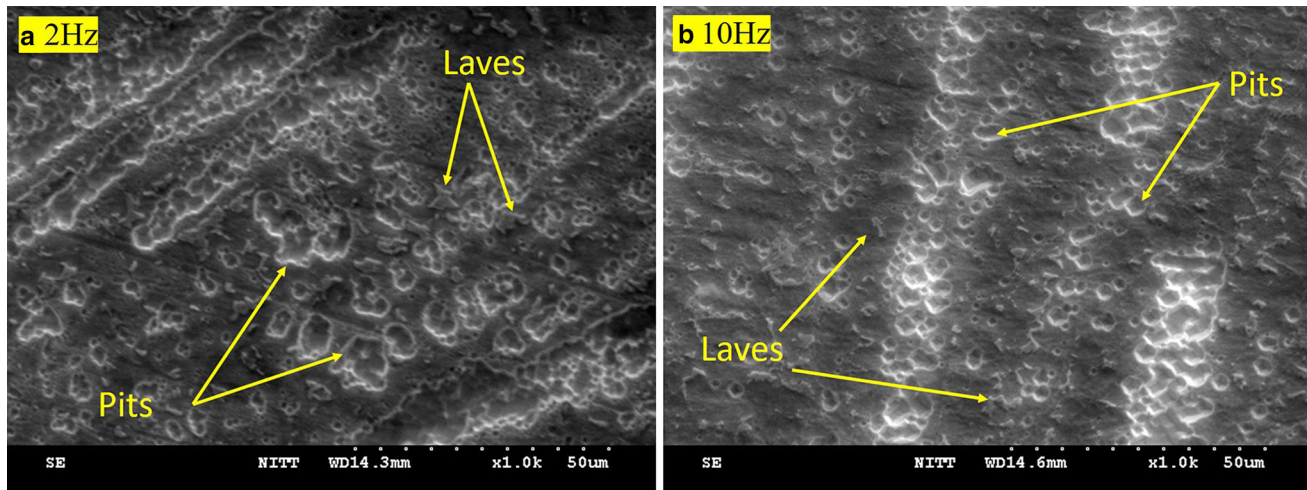


Fig. 17 Corroded surfaces of **a** 2 Hz and **b** 10 Hz observed through SEM

4 Conclusions

Microstructural and corrosion properties of pulsed GTAW are studied, and the following conclusions are arrived.

- Defect free welds were obtained by using Argon (95%) + hydrogen (5%)-shielding gas.
- The increase in pulse frequency reduced the weld bead width; however, the depth of penetration remained unchanged.
- Enhanced cooling rates at higher pulse frequency (10 Hz) favored for fine equiaxed grain growth than the lower pulse frequency (2 Hz).
- Laves fraction in the weld was reduced from 8.2 to 3.7% when the pulse frequency increased from 2 to 10 Hz.
- The pitting corrosion resistance was improved with an increase in pulse frequency due to lower laves segregation.

Acknowledgements The authors are grateful to the National Institute of Technology, Tiruchirappalli, India, and Vellore Institute of Technology, India, for supporting this research work.

References

1. Mirzaei M, Jeshvaghani R A, Yazdipour A, and Zangeneh-madar K, *Mater Des* **51** (2013) 709.
2. Janaki Ram G D, Venugopal Reddy A, Prasad Rao K, and Madhusudhan Reddy G, *Sci Technol Weld Join* **9** (2004) 390.
3. Wei P S, *J Heat Transf* **133** (2011) 031005.
4. Benea L, *5th IEEE Int Conf E-Health Bioeng* **5** (2015).
5. Lucas M J, and Jackson C E, *Weld J* **49** (1970) 46.
6. Mills W J, *Weld J* **63** (1984) 237s.
7. Lambarri J, Leunda J, García Navas V, Soriano C, and Sanz C, *Opt Lasers Eng* **51** (2013) 813.
8. Radhakrishnan C, and Prasad Rao K, *J Mater Sci* **32** (1997) 1977.
9. Hirata Y, *Weld Int* **17** (2003) 98.
10. Long Y, Nie P, Li Z, Huang J, Li X, and Xu X, *Trans Nonferrous Met Soc China* **26** (2016) 431.
11. McInerney T J, and Madigan R B, *Achieving Grain Refinement through Weld Pool Oscillation*, ASM International (2005).
12. Davies G J, and Garland J G, *Int Metall Rev* **20** (1975) 83.
13. Janaki Ram G D, Reddy A V, Rao K P, and Reddy G M, *J Mater Sci* **40** (2005) 1497.
14. Suresh M V, Vamsi Krishna B, Venugopal P, and Prasad Rao K, *Sci Technol Weld Join* **9** (2004) 362.
15. Manikandan D S, Sivakumar D, Kalvala P, and Kamaraj M, *Frequency Modulation Effect on Solidification of Alloy 718 Fusion Zone*, Materials Science & Technology (2013).
16. Reddy G M, Mohandas T, and Papukutty K K, *J Mater Process Technol* **74** (1998) 27.
17. Ishida T, *J Mater Sci* **23** (1988) 3232.
18. Becker D W, and Adams Jr C M, *Weld Res Suppl* **0** (1979) 143.
19. Kurzynowski T, Smolina I, Kobiela K, Kuźnicka B, and Chlebus E, *Mater Des* **132** (2017) 349.
20. Song Y, Shi H, Wang J, Liu F, Han E-H, Ke W, Jie G, Wang J, and Huang H, *Acta Metall Sin (English Lett)* **30** (2017) 1201.
21. Tusek J, *Int J Hydrog Energy* **25** (2000) 369.
22. Anbarasan N, Jerome S, and Arivazhagan N, *J Mater Process Technol* (2018).
23. ASTM International, *ASTM Int G59-97* (2014) 1.
24. Chen T, Nutter J, Hawk J, and Liu X, *Corros Sci* **89** (2014) 146.
25. Xiao Y H, den Ouden G, and Den Ouden G, *Weld J* **69** (1990) 289.
26. Andersen K, Cook G E, Barnett R J, and Strauss A M, *IEEE Trans Ind Appl* **33** (1997) 464.
27. Kotecki D J, Cheever D L, and Howden D G, *Weld J* **51** (1972) 368.
28. Valencia J J, and Quedsted P N, *ASM Handbook*, Vol. 15 Cast. **15** (2008) 468.
29. Cieslak M J, *Superalloys 718, 625 Var Deriv* (1991) 71.
30. Woo I, Nishimoto K, Tanaka K, and Shirai M, *Weld Int* **14** (2000) 514.
31. Manikandan S G K, Sivakumar D, Prasad Rao K, and Kamaraj M, *Mater Charact* **100** (2015) 192.
32. Vishwakarma K R, Richards N L, and Chaturvedi M C, *Mater Sci Eng A* **480** (2008) 517.
33. Yang M, Qi B, Cong B, Liu F, and Yang Z, *Int J Adv Manuf Technol* **68** (2013) 19.

34. Prifiharni S, Anwar M S, Nikitasari A, and Maburri E, in *AIP Conf Proc* (2018), p 020041.
35. Chen T, John H, Xu J, Lu Q, Hawk J, and Liu X, *Corros Sci* **78** (2014) 151.
36. Gooch T G, *Weld Res* (1996) 135 s.
37. Itman Filho A, Silva R V, Cardoso W da S, and Casteletti L C, *Mater Res* **17** (2014) 801.
38. Cardoso J L, Silva Nunes Cavalcante A L, Araujo Vieira R C, de Lima-Neto P, and Gomes da Silva M J, *J Mater Res* **31** (2016) 1755.

Publisher's Note Springer Nature remains neutral with regard to jurisdictional claims in published maps and institutional affiliations.